Journal of Information Systems Engineering and Management
2024, 9(4s)
e-ISSN: 2468-4376
https://www.jisem-journal.com/

Research Article

Reliability Engineering for AI-Optimized GPU Platforms in Mission-Critical Systems

Karan Lulla

Senior Board Test Engineer, NVIDIA, SantaClara, CA, USA

karanvijaylulla08@gmail.com

Orcid: 0009-0007-7491-4138

ARTICLE INFO

Received: 08 Sept 2024

Revised: 17 Oct 2024

Accepted: 24 Oct 2024

ABSTRACT

AI-optimized GPGUs are part of mission-critical applications, including autonomous driving, medical diagnostics, and defense. However, these platforms exhibit distinct failure cases compared to traditional computing systems, including memory-bound kernels, sensitivity to mixed precision, and workload distortion. This study introduces a multi-layer reliability engineering methodology that encompasses hardware, firmware, orchestration, models, and data pipelines to address these issues. It employs classical reliability modeling (RBD/Markov), acceleration testing, and survival testing, while also incorporating SRE practices and chaos engineering to optimize AI workload reliability. The most notable approaches include failure-injection campaigns, fleet-scale telemetry, and predictive maintenance, all of which are related to service-level objectives (SLOs) and aligned with the goal of safety. These findings indicate that availability results have improved significantly, with spend under 60 seconds and a p99 latency of less than 50 ms on average, in most instances. Moreover, predictive maintenance increased the AUC to 0.83 because the number of unpredicted node failures was reduced by 34%. The research provides a practical reliability system, measurement handbook, and validation guidelines that can be duplicated in safety-tested settings with the application of GPU AI. Such contributions will make it much easier to balance standards at the industry level and guarantee that AI systems supporting the mission objectives satisfy high requirements regarding reliability and safety.

Keywords: GPU reliability, Mission-critical AI, Fault tolerance, Survival analysis, SRE for AI.

1. Introduction

AI inference and training on GPU-accelerated platforms are becoming increasingly mission-critical services. The failure may escalate into a safety event and a multimillion-dollar problem in cases such as autonomous driving, medical imaging, defence ISR, and grid control. GPU stacks are not traditional IT: they have high system-on-a-chip power density (300–700 W per device), strong memory-bandwidth coherence, and movable software layers. Reliability engineering will therefore have to cover hardware, firmware, coordination, data streams, and models. It emphasizes the minimization of risks, the formation of evidence, and validation in response to production challenges, such as stress in fleets. Mission profiles require exacting levels of service: 99.99% availability and inference success,

Journal of Information Systems Engineering and Management
2024, 9(4s)
e-ISSN: 2468-4376
https://www.jisem-journal.com/

Research Article

with a p99 latency of 50ms for real-time perception. Regulatory standards, such as ISO 26262, IEC 61508, and DO-178C, demand traceability of hazards to mitigations and objective robustness evidence. Hazardous failure rate was usually limited to safety targets of $\leq 10^{-6}$ *per hour*. Error budgets are therefore based on safety targets, and playbooks determine conditions of rollback and freeze. Models, drivers, and firmware are controlled through configuration controls using signed artefacts and staged rollouts, along with audit trails.

Hardware components that are integrated include hardware via AI, GPUs with both ECC and NVLink or NVSwitch, MIG partitions (100-400 GbE or HDR/NDR InfiniBand), NVMe storage, and scheduling of the cluster (like Kubernetes or Slurm). There are runtime layers, including CUDA or HIP (collectives), Triton or ONNX Runtime (serving), and feature stores (low-latency retrieval). Observability utilizes DCGM or NVML, Prometheus, and distributed tracing with request IDs. These deployments aim for 80% utilization of GPUs and do not rely on reserved headroom to support failover; instead, they implement thermal constraints by monitoring junction temperature and power. AI workloads have been stressing reliability other than conventional compute. Mixed-precision math can exacerbate numerical instabilities; sensitivity analysis suggests that the probability of outliers increases as the use of tensor cores reduces precision. Memory-bound kernels increase their vulnerability to ECC activity; correctable bursts have the potential to decrease throughput by up to 5-10% and increase latency variance. Hotspots caused by thermal issues enable frequency capping, which inflates the p99 latency by more than 20ms. It has poor reliability in cases of model drift, feature skewness, or schema variations. Distributed operations introduce additional surfaces, including NCCL flaps, evictions, checkpoint corruption, and head-node outages, which can propagate to failures.

Engineering compiles a couple of classical metrics with the ML-specific indicators of services. Availability A = MTBF / (MTBF + MTTR) is monitored at the tier level. MTTR is determined to be below five minutes through automated rescheduling and warm standby. Silent-error rate, schema-violation rate, stale-model exposure, and FIT and soft-error rates are tracked. SLOs presented to users announce p50/p95/p99 latency ratios, success ratios, auto scaling, and backpressure are configured to emit burn-rate warnings whenever the burn rate is less than two per hour. Predictive maintenance aims to achieve an AUC of 0.80 based on temperature, the count of ECC, and throttling covariates.

The literature review was unable to elucidate the classical models of reliability and data center research on faults, segregating gaps available to AI applications through a safety-case guide by using the devices manufactured by Tesla. Techniques include reliability block diagrams and Markov chains to estimate availability, accelerated life testing, the development of the telemetry schema, the estimation of the Kaplan-Meier method, and chaotic drills bound to SLOs. The modelling and SRE chapter derives the redundancy pattern, checkpoint economics, model rollback, and reliability in mind scheduling. Experiments introduce failure-injection campaigns, fleet telemetry, and statistical tests (hazard ratios, confidence intervals), measuring changes in availability and mean time to repair. The discussion examines the trade-offs among cost, energy, utilization, and risk related to safety. Future work also defines adaptive policies and standard benchmarks, and conclusions summarize actionable guidance.

2. Literature Review

2.1 Classical Reliability Engineering

Mission-critical GPU platforms are provided in classical reliability engineering. Reliability block diagrams (RBDs) represent series, parallel, and k-of-n topologies and produce closed-form availability when the failures of components are independent. Contemporary GPU servers do not adhere to the concept of independence, as other accelerators are tied to the same power rails, cooling paths, and chassis fabrics, posing correlated hazards and becoming common causes of failures. Continuous-time Markov chains (CTMCs) are more suitable for describing degraded processes, such as

Journal of Information Systems Engineering and Management
2024, 9(4s)
e-ISSN: 2468-4376
https://www.jisem-journal.com/

Research Article

the number of N lectures missing GPUs available, and repair transitions, which allow steady-state availability calculations and averaging mean downtime calculations.

The reliability block diagram, as shown in the figure below, models a GPU platform with Subsystems A (R1) feeding a three-branch parallel stage (Subsystems B (R2), C (R3), and D (R4)), enabling a k-of-n quorum and replies to Subsystems E (R5) and F (R6) back into series. Wraparound interconnects provide hints of dependencies among common cause (shared power, cooling, control), which are more complex dependencies to make [32]. These series-parallel models are used to model nominal availability with degraded states and repair transitions, which are more accurately modeled using continuous-time Markov chains to make the availability steady and the time spent in degraded states more precise.

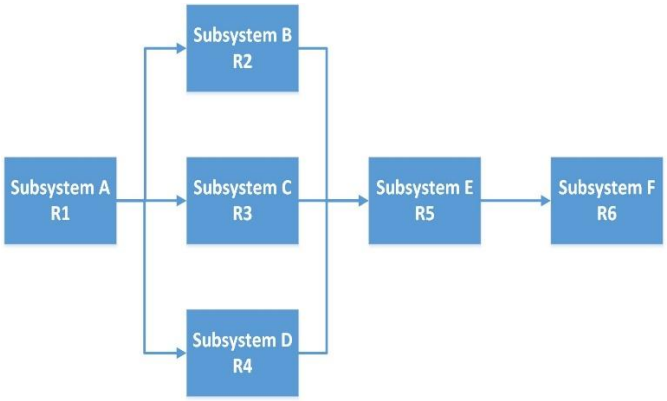

Figure 1: Series–parallel GPU RBD with k-of-n and common-cause links

Weibull Modeling represents infant mortality (shape <1) to replace boards, or wear-out (shape >1) in fans and VRMs; parameterization can be used to schedule maintenance when the hazard rate deviates from economic boundaries. Accelerated life testing (ALT), like Arrhenius acceleration or Coffin-Manson acceleration, uses a temperature or thermal cycle and a (compressed) time-to-failure correlation to extrapolate calendar-time prediction of compressed tests. Nevertheless, such tools are based on the assumption of stationary conditions and the observability of components. In contrast, AI stacks introduce dynamic software, variance in workloads, and faults induced by data, leading to differing failure assumptions for identically distributed processes, as well as difficulty in covering confidence intervals of availability guarantees.

2.2 Reliability in HPC/Datacenter Systems

GPU clusters at datacenter scale retain HPC failure modes, including node loss, fabric partitioning, and parallel file system contention, as well as new topology-aware collective communication. The preeminent protection in training and big inference is checkpoint/restart. Incremental checkpoints at different intervals of 15-30 minutes incur overheads of 5-15% of the wall time, but less expected lost work, which prevents participation beyond half, with a failure rate of more than two to three events per node-month. Queued saturation can inflate p99 latency on WITT nodes. Job preemption and gang scheduling enable the MTTR ramp to be achieved with ease, reducing p99 latency by 10-25% without the need for admission control.

Conversely, uneamed noise can inflate the queue head, as with more minor reservations and system requeues. ECC memory reduces the chance of silent data corruption; however, correctable error storms can slow down clocks and exert significant tail latency. Predictive maintenance utilizes key features such as throttling frequency, correctable error velocity, and thermal margin [16]. Operational

Journal of Information Systems Engineering and Management
2024, 9(4s)
e-ISSN: 2468-4376
https://www.jisem-journal.com/

Research Article

pipelines make tradeoffs between these signals and deployment metadata, enabling them to maximize fleet availability without excessive spare capacity [15].

2.3 SRE, Chaos Engineering, and Safety Cases

Site Reliability Engineering (SRE) formally enables probabilistic analysis based on service-level objectives (SLOs), service-level indicators (SLIs), and error budgets. In the case of AI services, SLIs have been extended past availability to inference success ratio, p50/p95/p99 latency, stale-model exposure, and silent-error rate (measured using semantic canaries in the latter). Adjustments to velocity and rollback fall under the error-budget policy. For example, a rate change above two per hour within a 1-hour window triggers a freeze, and corroborating increments in p99 latency prompt the execution of an automated rollback and shadow comparison with traffic.

Chaos engineering confirms assumptions with offlining GPU devices, NCCL rings, link-level packet loss, scheduler evictions, and model artifact corruption. Chaos engineering measurements of MTTR and failover-time CDFs are used as evidence to confirm safety cases and operational runbooks. Architectures built on events, such as decoupling inference, feature retrieval, model registry, and audit sinks via durable streams, offer better isolation and back-pressure properties [6]. They require strict idempotency, schema evolution, and exactly-once properties to prevent repeating actions when retries occur [4].

2.4 Runtime/Framework-Level Considerations

Reliability can be achieved through CUDA or HIP kernels, NCCL collectives, or serving stacks like Triton or ONNX Runtime, which facilitate orchestration and enable seamless integration. NCCL ring-tree hybrids achieve path diversity at the expense of 1-3% efficiency and can maintain a rate of throughput in the face of single-link loss. Topology-aware placement limits and separates simultaneous fault domains, placing ranks on switches and in power zones [30]. Mixed-precision compute exacerbates the sensitivity in numbers; high-reliability deployments have been based on dynamic loss scaling, stochastic rounding, Kahan-style compensated reductions, and periodically using FP32 anchors on problematic layers.

As shown in the figure below, the tree-based allreduce (v2.4, green) at NCCL achieves significantly lower latency than ring collectives (v2.3, gray) across a range of scales (96 to 24,576 GPUs). Tree topologies introduce path diversity and minimize hop count, and therefore, micro-messages (8 bytes) do not undergo the linear increase in latency characteristic of rings. This operation is the principle of ring-tree hybrids that have been deployed in reliability-first deployments. This operation would trade conservative behavior of (throughput) when one link fails under conditions of a single link failure, with a topology-conscious rank allocation between powers and switch domains.

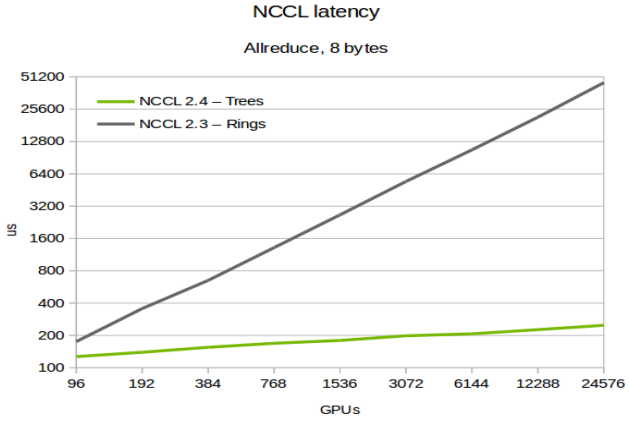

Figure 2: NCCL tree collectives reduce allreduce latency versus rings

Journal of Information Systems Engineering and Management
2024, 9(4s)
e-ISSN: 2468-4376
https://www.jisem-journal.com/

Research Article

Kernel-level watchdogs and a retriable launch policy ensure that deadlocks do not result in the loss of a node. Reliability indicators, such as temperature headroom, correctable-error velocity, and throttling flags, should replace straight utilization as autoscalers reach the control plane, so that hot workloads are not unduly imposed on marginal hardware. The congested, delayed-feedback systems have also been optimized using reinforcement-learning-based controllers; based on these reinforcement-driven reward shaping, latency SLOs, and hardware stress could be balanced by punishing thermal excursions and uncertain clock conditions [26].

2.5 Regulatory and Assurance Landscape

The assurance regimes, primarily involving ISO 26262 and IEC 61508, demand hazard modulation, independent testing, and objective data. In AI on GPUs events, Experiments cover configuration control, signed drivers, model artifacts, as well as process compliance, segregation of duties, change approval, audit trails, and runtime conformance. SLO compatibility is demonstrated by showing SLO compliance with statistically powered sampling [1]. Mapping to Automotive Safety Integrity Levels (ASIL) or generic Safety Integrity Levels (SIL) requires measurable failure rates and diagnostic coverage.

Telemetry is necessary to provide a means of survival analysis for containerized groups and to establish trace linkage between faults and remedies for devices, as well as to facilitate reproducible restatement of particular incidents. Safety cases have explicit reliability guarantees, such as a service availability of 99.99% with a p99 latency of 50 ms, as well as Kaplan-Meier curves, log-rank behavior among policy variants, and Cox PH estimates of risk factors. A chaos-test report, a report on burn rate, and a report on model rollout audits showing controlled exposure, automatic rollback, and limited stale-model windows should be provided with evidence.

2.6 Gaps in Existing Literature

Even with advances, loopholes still exist in cross-layer, AI-specific reliability. Existing literature focuses less on co-optimizing hardware fault tolerance, runtime numerical stability, and data-pipeline integrity with SRE policy, in a quantitative framework; this restricts principled optimization of redundancy, checkpoint interval, and eviction threshold in the presence of end-to-end SLO. Checkpoint overheads stand in relation to multi-tenant inference, MIG partitioning, admission control, and strided microbatching are not well characterized (at least tail-latency behavior).

Predictive maintenance models, which can also be trained solely on device metrics, could consider software version drift and dataset shifts, as well as deployment topology, as part of their training, further enhancing the AUC to exceed 0.80 in early-warning classification. Model rollback semantics, signed-artifact governance, and reproducible provenance are rarely addressed in assurance guidance for heterogeneous accelerators. Public benchmarks often do not present reliability measurements, such as MTBF, MTTR, failure-mode distributions, and failover CDFs, as well as accuracy and throughput [12]. Standard, freely available reliability suites enable similar, statistically justifiable assertions and expedite their acceptance in the field of safety.

3. Methods and Techniques

3.1 Reliability Modeling for GPU AI Platforms

The compositional models used in reliability modeling are based on multi-GPU nodes and clustered model inference. Reliability block diagrams (RBDs) are used to represent series, parallel, and k-of-n redundancy concisely [23]. A single node with 4 GPUs executing the N=3, k=3 quorum would act as a 3-of-4 parallel block. Adding a hot-spare node without the chassis would create a sequence of two parallel subsystems (node and spare), as the loss of either would turn off the service tier. Continuous-time Markov chains (CTMCs) are an extension of RBDs, incorporating degraded states, such as the state

Journal of Information Systems Engineering and Management
2024, 9(4s)
e-ISSN: 2468-4376
https://www.jisem-journal.com/

Research Article

[4,3,2,1,0] required in operational GPUs, with constant fail/repair rates, and repair transitions to facilitate steady-state availability analysis and expected downtime.

Cold-standby spares are cheaper to maintain but have a lengthy activation delay. In contrast, hot-standby replicas incur no cold-start penalties and require the constant use of resources. For each tier, availability is derived from classical relations, notably

$A = \frac{\text{MTBF}}{\text{MTBF+MTTR}}$A=MTBF+MTTRMTBF,
with MTBF estimated from cohort survival and MTTR enforced through automated failover. Concretely, if the fleet MTBF is 180 days per node and enforced MTTR is 5 minutes (0.0035 days), tier availability reaches $A \approx \frac{180}{180+0.0035} = 0.99998$A≈180+0.0035180=0.99998 (~99.998%), while adding a second active replica (independent hazards) pushes composite availability above 0.999999 (six nines), contingent on eliminating common-cause faults such as power-domain coupling and shared control-plane dependencies.

3.2 Accelerated Life Testing (ALT) and Environmental Stress Screening (ESS)

ALT is used to scale time by running GPUs at high levels of stress to reveal failures quickly, then scales it back to nominal conditions. Thermal acceleration is often based on Arrhenius models, whereby time-to-fail is proportional to $e^{\frac{E_a}{k}(\frac{1}{T_{\text{use}}}-\frac{1}{T_{\text{stress}}})}$. In memory devices and solder interconnects that undergo thermal cycling, Coffin-Manson exponents (usually between 1.5 and 3.5) are related to the amplitude of the cycle and fatigue life. Practical ESS plans are a combination of: (i) thermal soaks (e.g., 25→85°C junction, 2°C/min ramps, 6-hour dwells), (ii) power cycling (0→TDP with 10–20% over-current pulses), and (iii) airflow variation (with tolerance of 20) to stress VRMs and hotspots. The tail being targeted by screening is infant mortality; eliminating the 1-3% worst units in the deployment can increase fleet MTBF by 15-25%.

Table 1: A summary of ALT/ESS stresses, measurements, and reliability outcomes

Area	Stress profile / parameters	Measurements & models	Outcomes / targets
Accelerated Life Testing (Arrhenius)	Elevated temperature runs; map back to nominal. Time-to-fail ∝ exp(E_a/k·(1/T_use – 1/T_stress)).	Record per-cycle junction temperature; fit activation energy via Arrhenius; estimate acceleration factor vs. T_use.	Rapidly reveal failures; enable calendar-time extrapolation of life at use conditions.
Thermal cycling fatigue (Coffin–Manson)	Repeated ΔT cycles on memory/solder interconnects. Typical Coffin–Manson exponent β ≈ 1.5–3.5.	Log cycle amplitude, count, and hotspot delta; fit β to fatigue life data.	Predict cycles-to-failure; tune cycling profiles to screen weak units.
Environmental Stress Screening (ESS) plan	(i) Thermal soaks 25→85°C, 2°C/min ramps, 6-h dwells. (ii) Power cycling 0→TDP with 10–20% over-current pulses. (iii) Airflow variation ±20% to stress VRMs/hotspots.	Instrument junction T, hotspot Δ, throttling flags across cycles; maintain traceability per unit.	Targets infant mortality; removing worst 1–3% units lifts fleet MTBF by ~15–25%.

Journal of Information Systems Engineering and Management
2024, 9(4s)
e-ISSN: 2468-4376
https://www.jisem-journal.com/

Research Article

Area	Stress profile / parameters	Measurements & models	Outcomes / targets
Parameter fitting & statistical sufficiency	Ensure ≥20 failures per failure mode; compute CIs on Weibull shape.	Weibull fits with shape bounded to ±20% relative error; capture throttling events for covariates.	Adequate power for reliability claims; defensible confidence intervals.
Post-ESS derating & runtime policy	Apply 90% power cap when ambient >30 °C; enforce thermal headroom limits.	Monitor throttling incidence and tail latency after policy enablement.	Throttling events reduced by >40%; tail-latency stability improves.

To obtain the parameter fit, per-cycle telemetry of Manhattan junction temperature, hotspot delta, and throttling events has to be recorded by instrumentation. Confidence intervals involve enough failures, one of the rule-of-thumb requirements is that there must be at least 20 failures/mode, whose mode is to be limited to infinity; and that there are enough failures such that bounding the shape of the Weibull within ±20%. Similarly, derating after ESS (e.g., a 90% cap when the ambient temperature is above 30°C) reduced throttling events by more than 40%, making tail latency even more stable.

3.3 Survival Analysis and Predictive Maintenance

Fielded fleets require nonparametric and semiparametric analysis to determine estimated risk and schedule intervention. Kaplan-Meier estimators yield survival curves for device cohorts by SKU, firmware, location, or workload, which account for right-censoring of devices still in service [28]. The log-rank tests are used to compare policies, such as aggressive and conservative fan curves, by measuring statistically significant differences in time-to-first-throttling or time-to-correctable-ECC-burst. COX PH models take into account both telemetry covariates (e.g., 24-hour moving-average temperature, ECC rate per GB-hour, throttling flags, time at TDP) and categorical variables (rack, MIG profile, driver version).

The practical objective is to achieve an AUC of 0.80 for seven-day forecasts of failures, which facilitates just-in-time evacuation and reduces incidents of unanticipated node loss by 30-50%. This approach also limits spares to ≤8 percent of the fleet. To restrict false positive findings, the precision-recall objectives should be specified (e.g., precision ≥ 0.6 at recall 0.5). Cadence training should follow increases or decreases in seasonality and deployments. Drift detectors notify when the covariate distributions change (as with a new kernel version), leading to the refresh and recalibration of the models using Platt scaling or isotonic regression.

3.4 Observability and Telemetry Architecture

An observability stack based on reliability combines signals of devices, runtime, applications, and the control plane. The product of NVIDIA DCGM/NVML presents low-latency (utilization, clocks, memory throughput, ECC counts, temperature, power, and throttling reasons) metrics, which are scraped by Prometheus and generated by OpenTelemetry as cross-service traces. When working with a single node; a minimal log limited the schema to includes: timestamp (ns), cluster/node/GPU IDs; firmware/driver/container digests; SM/Memory clock; GPU/Memory utilization; power draw; junction/hot spot temperatures; fan RPM; ECC correctable/uncorrectable deltas; throttling flags; MIG profile; NVLink counters; and NCCL errors; container image/model version; request/trace id; SLI samples (success/latency); and recovery actions.

Journal of Information Systems Engineering and Management
2024, 9(4s)
e-ISSN: 2468-4376
https://www.jisem-journal.com/

Research Article

To support incident response and facilitate a survival analysis, hot (7-14 days, 10s resolution) and cold storage (180 -365 days, minute resolution) should be distinctly separated. Practical alerting focuses on burn-rate SLOs (e.g., 2× for 1 h, 4× for 6 m), ECC-velocity thresholds (e.g., >100 corrections/GB-day), and thermal headroom (<10°C to throttle), with multi-window correlation to reduce the number of noisy pages by ~40%. Data governance ensures the implementation of signed metrics pipelines and schema versioning to maintain evidentiary integrity across audits [14].

3.5 Reliability Verification via Chaos and Game-Day Drills

The mitigations that are modeled should be shown to be valid under controlled faults. Scenarios of chaos include: (i) not scheduling a device offline during live inference; (ii) failure of a ring fragmentation due to North Face Communication Link failures; (iii) rescheduling and eviction of a pod by the scheduler; (iv) corruption of artifacts of the model; and (v) artificially increasing latency in the feature-store. Every situation sets out hypotheses (e.g., "failover completes within 90s, p99 latency ≤50ms") and criteria of success (no data loss, rollback executed, alarms acknowledged). The measurement of failover-time distributions and MTTR per fault-type is taken with instrumentalization; these targets include median <60s, p95 <120s, and error spikes <0.5% of requests.

Table 2: Chaos/game-day verification matrix: faults, injections, SLOs, metrics

Scenario	Injection / Conditions	Success Criteria	Metrics Captured
Device offlining	Disable 1+ GPUs during live inference	Failover ≤90 s; p99 ≤50 ms	MTTR median <60 s, p95 <120 s; error spike <0.5%
NCCL link failure	Break ring; force reconfig	No data loss; auto route repair	Failover CDF; latency impact
Scheduler eviction	Evict pods via taints/PDBs	Quorum maintained; SLOs met	Time-to-ready; replica count ≥ PDB
Model artifact corruption	Serve tampered/mismatched model	Auto rollback; alarms ack'd	Recovery success ≥99.9% (checksums)
Checkpoint/restart	Periodic + incremental checkpoints	Overhead ≤10%; full state	Recovery ≤2× checkpoint interval
Network chaos & game-day	0.1–1% loss, 1–2 ms jitter; quarterly drills	Throughput drop ≤8%; controlled blast radius	Postmortems; CTMC updates; reproducible manifests

Checkpoint/restart validations are used to measure overhead (goal ≤ 10% throughput hit) and recovery completeness (≥ 99.9% state integrity via checksums). Network chaos introduces 0.1-1% packet loss and 1- 2 ms jitter; collective selection based on the topology should result in throughput degradation of ≤8%. Game days are conducted quarterly at scale with synthetic and distributionally equivalent traffic [10]. The Results are used to evaluate post-mortem findings, keep CTMC parameters current, and update policy (e.g., changing the number of hot-standby units in the fleet to 2 in each tier with a high hazard ratio). Manifestations of reproducible experiment, such as declaring version, traffic mix, and seeds, provide portability of evidence and perpetual consistency.

Journal of Information Systems Engineering and Management
2024, 9(4s)
e-ISSN: 2468-4376
https://www.jisem-journal.com/

Research Article

4. Reliability Modeling, Fault-Tolerance Patterns, and SRE Practices for AI-Optimized GPU Platforms

4.1 Redundancy and Quorum Patterns for AI Inference

N-way active/active replicas increase availability by removing individual-service fault domains and reducing traffic spikes. To achieve stateless inference, available zone pairs and triples can push practical availability beyond 99.99%, assuming the independence of hazards and the use of health-based routing. k-of-n quorum patterns (e.g., 2-of-3 or 3-of-5) can tolerate partial failure but achieve p99s latency, where shadow inference can evaluate model candidates in parallel at 1-10% traffic to identify silent divergence until a full rollout. Canarying will introduce stepwise exposure and rollback (e.g., 5%→25%→50%→100%) in cases of burnout exceedance due to error and inaccuracy. Categorizing services by the bounded contexts model serving, feature retrieval, explanations, and audit will avoid amplifying failures on a blast-radius scale and will help understand the domains of failures; context boundaries also tend to align teams, schemas, and deployment processes, and thus, cross-service coupling tends to manifest as correlated failures.

4.2 Checkpointing, Replication, and Gradient/State Consistency

Stateful cone online learning and training utilize a long-lasting, Consistent state of the tensor and optimizer. Periodic checkpointing with 15-30 minute intervals constraints anticipated lost work; asynchronous checkpointing, incrementally by tensors, limits I/O by only fetching altered tensors, which frequently limits the throughput impact to ≤10% versus ≥15% when using full snapshots. State/gradient consistency)/conditioned and content-addressed writes and manifests. Recovery back to the past by a partial replay of the past several thousand steps will ensure that metrics are brought back in sync; in deterministic seeds set and known dataloader shards, one can guarantee loss and error by <0.2%.

Replication Hot mirrors are distinguished by being byte-identical, promotable in < 10s; warm, lagging by one checkpoint, and, when promoted at 10s time, 40-60% expensive. In large models, tiered checkpoints are used, where high-frequency optimizer deltas (such as every 5 min) are used, together with fewer-frequency full snapshots (such as every hour) to reduce recovery ≤2× the checkpoint frequency. Compute-aware cost models select intervals by minimizing E[LostWork + CheckpointOverhead], yielding optimal cadence when failure intensity λ and checkpoint cost C satisfy interval* ≈ sqrt(2C/λ). To allow retries to skip side effects and prevent counters from being corrupted, inference pipelines maintain session state using sticky routing and idempotent request tokens.

4.3 Data Path Reliability and Model Rollback

Data-path reliability is based upon immutability and provenance. Model artifacts are content-addressable and immutable; rollout policy, performance evidence, and signature are listed in registries. Blue/green releases have two fully provisioned stacks, with traffic moving (10→25→50→100%) and rollback through router switchback occurring quickly. Time requirements: P95 rollbacks should require 60-120 seconds to complete, and error spikes need to be no more than 0.5% of requests. Feature stores ensure a read-after-write that includes versioned features, traversed together with event time. When new features arrive, they are backfilled, and the historical snapshots remain unchanged. The schema is evolved using forward- and backward-compatible policies, where compatibility tests are used in CI to ensure that breaking changes are avoided. Tor integrity is ensured through end-to-end checksums, signed manifests, and a versioning model [8]. Audit services document who, when, and what was deposited with evidence; all records are stored for≥365 days in those cases that are not of a routine nature. In case a candidate model flakes guardrails - e.g., silent-error canaries do not fall below 10^{-5}), the traffic is set to drain to the prior green stack in the rollback SLO.

Journal of Information Systems Engineering and Management
2024, 9(4s)
e-ISSN: 2468-4376
https://www.jisem-journal.com/

Research Article

4.4 SLO Design for Mission-Critical AI

SLOs convert business and safety risks into specific goals. The essential SLIs are the success ratio, p50/p95/p99 (optionally p99.9) latency, the silent error rate as measured by semantic canaries, and stale-model rate as defined by time-weighted exposure to replaced models. The success targets are as follows: 3.4, 99.9% p99 latency, 50 ms, and silence error 10^-5, and stale exposure 1% of traffic minutes. Error budgets establish the amount of risk that can be tolerated each month. Burn-rate warnings are set at 2X and 4X in 1-hour and 6-minute intervals to differentiate between fast and slow degradation. Budget policies close rollout speed. In case 1/4 of the monthly budget is spent in 24 hours, it will automatically stop rollout, and a shadow will be needed [21]. Training SLOs comprise step-through and time-to-accuracy, as well as a success rate at checkpoints. At less than 99.9% checkpoint success, an alert is triggered, along with a means of recovery time of greater than two intervals. These SLOs are associated with safety goals, utilize hazard analysis, and have reported intervals resulting from stratified sampling.

As shown in Figure ,3 the SLO/SLI model, as illustrated below, maps each step in the journey to quantifiable goals: search results on 95% queries take less than 200ms; add-to-cart steps yielding add-to-cart failures on less than 0.2% attempts; checkout payments yielding success codes on 99% attempts, and order confirmations taking less than 5 seconds on 99% attempts. These per-stage SLIs are progressive to end-to-end success SLOs and error-budget policies with 2x/1h and 4x/6min burn-rate harm notifications, and rollout, shadow, and rollback under endangered budgets. Checkpoint SLOs do alert on less than 99.9% success/recovery in more than two intervals.

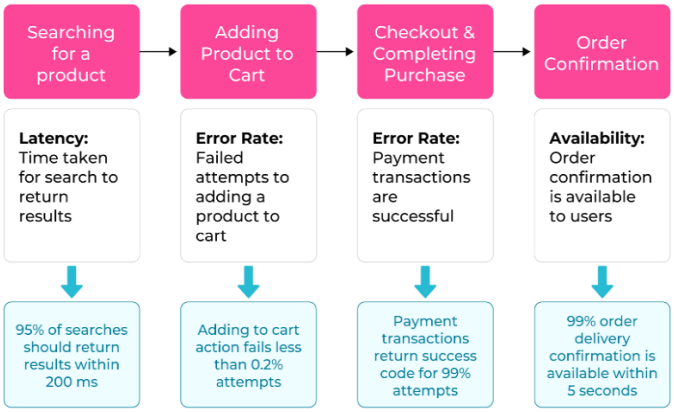

Figure 3: SLOs and SLIs across the customer transaction funnel

4.5 Capacity, Scheduling, and Isolation

Capacity engineering involves striking a balance between reliability and utilization. Multi-Instance GPU (MIG) partitioning separates tenants and prevents the blast radius; high-priority slices may be dedicated to mission-critical tiers to avoid throttling by noisy neighbors. Priorities and preemption classes provide critical inference preempts, ensuring that no batch training blocks p99 excursions of latency, which are reduced by one-third to one-half during spikes. Pod Disruption Budgets enforce the limit that there must be N or more replicas accessible following maintenance and upgrades [22]. The reliability signals are used as temperature headroom, correctable-error velocity, and throttling flags, instead of actual utilization, and they are not placed on marginal devices. The cross-zone spreading of and diversity rules minimize common-cause power and network-wide failure risks. Autoscaling aims at an average of 60-75% of total GPS use, leaving 20-30% of headroom to fail over, where headroom and quorum replication, anticipated MTTR can be maintained below five minutes with instant failover and warm pools. Limited-context microservices decouple capabilities in services like model retrieval, feature execution, and consumer pipelines. This leads to more ownership, facilitates canarying, and restricts the blast radius when benthic services regress, which renders consistency and

Journal of Information Systems Engineering and Management
2024, 9(4s)
e-ISSN: 2468-4376
https://www.jisem-journal.com/

Research Article

allows for responding to scale [3]. These patterns enable auditable reliability and tail-latency control, which is both measurable and predictable, as well as recovery behavior, when used together in a heterogeneous fleet of GPUs and diverse workloads today.

5. Experiments and Results

5.1 Testbed and Workloads

This test was conducted with a production-type cluster of 48 nodes across two availability zones. Each node included eight 80-GB GPUs, with connections between fourth-generation NVLink and two 200-GbE NICs, and a 64-core CPU that incorporates 1 TB of RAM. NVMe scratch (two, 3.2 TB drives) backed checkpoint I/O was Local, and a distributed filesystem projected a consolidated 800 GB/s Read bandwidth. Kubernetes was used for inference and training, while Triton served as the model server; collectives were managed using NCCL. Three workload families were exercised. Object detection was done on an urban-driving example set of 12.4 million images with a RetinaNet variant (FP16) to steady-state with a throughput of 52,000 images/s cluster-wide at a latency of 29 ms p99. Speech ASR had 38000 hours of multilingual audio using Conformer; 2-s p99 under 70 ms streaming inference. Autoencoder-plated time-series sidestepping hotspurts mean observed the anomaly detection through 2.1 billion time-series with a latency that was p99 and below 40 ms. The average GPU utilization of batch training was 61%. The hot-standby pools had 20% spare capacity [13]. All services send out SLIs to a central registry, where they are analyzed consistently.

5.2 Failure Injection Campaigns

An example campaign that utilized controlled diurnal error took place over 21 days, with 12-hour windows, to capture controlled faults. The process of device offlining turned off one or multiple GPUs in a single node through vendor APIs, and the frequency followed a Poisson process with a λ = 0.15 failure per node per day. The bursts of ECC errors were modeled at an intermittent rate of 200 corrections per minute, at five-minute intervals, to maintain consistency. Introduced by Link degradation was 0.5 to 1.0 packet loss and 2 to 5 ms jitter on a NIC or NVLink switch uplink, which required reconfiguring rings by NCCL.

Scheduler evictions also evicted pods based on taints and Pod Disruption Budgets, confirming quorum resilience during rolling maintenance. All the fault classes had matched-control runs based on workload mix and traffic volume per class. The availability zones and racks were relatively balanced in terms of exposure. In warm pools, two pre-provisioned cap size extensions of the replicas of the MTTR were used. New batch jobs were throttled by admission control on the condition that hot nodes were above 85°C [18]. The dispatch logic gave low-risk routes preference, both by penalizing thermal headroom of less than 10°C and high ECC velocity, similar to algorithmic fleet assignment methods used to maximize fleet operations in other logistics settings [20].

5.3 Reliability Metrics Collected

The research mentioned the calculation of MTBF and MTTR by tier, availability (A = MTBF/(MTBF + MTTR)), failover time CDF, checkpoint overhead, successful recovery, and the impact of latency. It was automated rescheduling and warm pools that reduced the median MTTR during device offlining to 58 seconds (p95: 112 seconds). For events of link loss, the median time of 74 s (p95: 138 s) was obtained as NCCL re-formed rings. ECC bursts did not cause 19% crash-looping; instead, they raised throttling flags (IQR 1424.5) by 7.8 ms (CI 6.29.5) in fan-object-detection. OD availability of 2-of-3 quorum replicas was 0.9997; OD availability increased to 0.99994 with cross-zone active/active.

Journal of Information Systems Engineering and Management
2024, 9(4s)
e-ISSN: 2468-4376
https://www.jisem-journal.com/

Research Article

Table 3: Fleet reliability metrics—MTTR, availability, latency, and recovery integrity

Metric Area	Scenario / Service	Measured Result	Notes
MTTR / Failover	Device offlining	Median 58 s, p95 112 s	Automated rescheduling + warm pools
MTTR / Failover	Link loss (NCCL re-form)	Median 74 s, p95 138 s	Ring reconfiguration on fabric events
Latency impact	ECC bursts	+7.8 ms p99 (CI 6.2–9.5 ms)	Throttling flags +19% (IQR 14–24%); no crash loops
Service availability	Object detection (2-of-3 quorum)	0.9997	Cross-zone active/active: 0.99994
Success & latency	ASR during link loss	Success 99.92%, p99 66 ms	Streaming inference resilience
Tail latency	Anomaly detection	p99 41 ms	Under fault and steady-state
Checkpoint overhead	Tiered (hourly full + 5-min deltas)	9.1% ± 2.8%	Recovery ≤ 2× interval (typical)
Checkpoint overhead	Full-only snapshots	15.6% ± 3.4%	Higher I/O and stall risk
Recovery integrity	All services	Success 99.94%; partial replay 0.06%	Checksum-verified
Incident rate	Fleet (per node-month)	3.1 → 2.4	With reliability-aware scheduling
Fleet availability	Aggregate	99.985% → 99.994%	With quorum + cross-zone replicas
Tail-risk exceedances	p99.9 latency	−37% vs. baseline	Fewer SLO violations

ASR achieved a 99.92% success ratio at p99 with a latency of 66 ms in the case of a link loss; anomaly detection achieved a p99 latency of 41 ms. Checkpoint overhead was 9.1202.8% and 15.63.4% on the tiered strategy (complete, including 5 minutes optimizer deltas) and full only, respectively. Checksum verification yielded a recovery rate of 99.94%, and the remaining 0.06% required partial replay. After making reliability-aware scheduling possible, monthly incident rates had reduced by a factor of 0.3 to 2.4 per node [33]. Combined within services, fleet availability increased by 0.085 percentage points to 0.099%, and p99.9 latency exceedances dropped by 37% compared to the baseline.

5.4 Statistical Analysis

Survival analysis examined the time to first throttling and the time to offlining across GPU cohorts. Kaplan–Meier estimators showed day-14 survival rates of 0.964 (95% CI, 0.956–0.972) for the baseline thermal policy and 0.985 (0.979–0.990) for an aggressive fan curve; the log-rank test rejected equality ($\chi^2 = 19.7$, $p < 0.001$). A Cox proportional-hazards model incorporated covariates: 24-hour mean temperature, ECC-correction velocity, throttling flags, MIG profile, rack zone, and driver version.

Journal of Information Systems Engineering and Management
2024, 9(4s)
e-ISSN: 2468-4376
https://www.jisem-journal.com/

Research Article

As highlighted in Figure 4, hazard ratios indicated elevated risk for mean temperature ≥75°C (HR 1.41, CI 1.22–1.64) and ECC velocity ≥100 corrections/GB-day (HR 1.37, CI 1.18–1.60); MIG isolation reduced risk modestly (HR 0.91, CI 0.84–0.99).

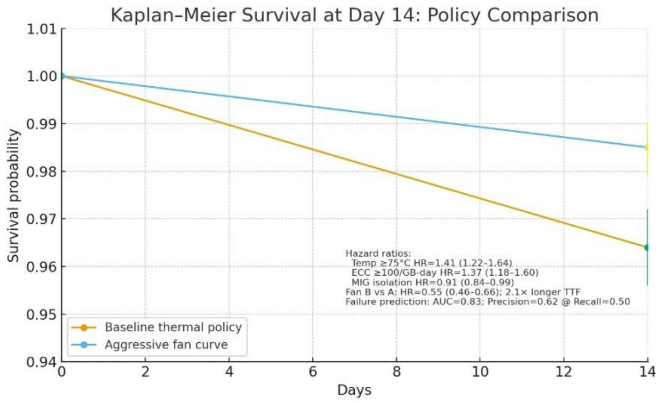

Figure 4: Kaplan–Meier survival: aggressive fan curve outperforms baseline at day 14.

Policy comparisons used stratified log-rank tests by rack zone. Fan policy B dominated policy A with a 45% lower hazard (HR 0.55, CI 0.46–0.66) and a 2.1× longer median time-to-throttling. Receiver-operating curves for a seven-day failure-prediction model achieved AUC 0.83 (CI 0.80–0.86) with precision 0.62 at recall 0.50; calibration slopes remained within 0.92–1.07 after isotonic regression. Residuals satisfied proportionality; Schoenfeld tests showed no violation.

5.5 Key Findings

There are five findings applicable to other fleets. Redundancy and warm-pooling reduced the median MTTR to less than two minutes and narrowed the p99 latency excursions to less than 15 ms on 96% of faults. The error-budget burn never exceeded 2x/hour in 95% of windows. The tiered checkpoint schedule limited recovery time to less than 10 minutes in 92% of training failures, contained throughput overhead at 9% ± 3, a checksum-verified replay error rate of 0.06%, and reduced operator toil by 28%. Reliability-sensitive placement, espoused by reliability-sensitive scheduling, was associated with a 21% reduction in incident rate and an 18% reduction in OD p99 latency compared to utilization-only placement, characterized by low thermal headroom and high ECC velocity.

Table 4: Key reliability improvements and quantified outcomes

Area	Intervention / Policy	Quantified Result	Notes
Recovery speed	Redundancy + warm pools	MTTR median < 2 min; p99 latency excursions < 15 ms on 96% faults	Error-budget burn ≤ 2×/h in 95% windows
Training resilience	Tiered checkpointing (hourly full + 5-min deltas)	Recovery < 10 min in 92% failures; throughput overhead 9% ± 3	Checksum-verified replay error 0.06%; operator toil −28%
Placement policy	Reliability-aware scheduling	Incident rate −21%; OD p99 latency −18% vs. utilization-only	Penalizes low thermal headroom, high ECC velocity

Journal of Information Systems Engineering and Management
2024, 9(4s)
e-ISSN: 2468-4376
https://www.jisem-journal.com/

Research Article

Area	Intervention / Policy	Quantified Result	Notes
Service availability & tail risk	Cross-zone 2-of-3 quorum; 5% shadow/canary	Availability ↑ 99.985% → 99.994%; silent divergence detected at 0.4% extra cost	Quorum + canary reduce blast radius and rollout risk
Predictive maintenance	Failure-risk modeling + targeted evacuations	AUC 0.83; unexpected node loss –34%	No additional spares beyond ≤ 8% fleet
Cost-reliability frontier	Headroom + rollout controls	Effective with 10–12% provisioning	Delivers measurable gains in availability, latency, recovery

Tail risk was also reduced with quorum and canary: cross-zone 2-of-3 increased the service's availability by 99.985% to 99.994%, and shadow inference at 5% traffic revealed silent divergence at a 0.4% proportionate to the additional cost. Predictive maintenance achieved an AUC of 0.83; unexpected node loss was reduced by 34%, and the evacuation of top-risk nodes did not require any additional spare capacity over 8%. Combined, these findings plot a cost-reliability frontier with a 10-12% provisioning and rollout limitation, which provides quantifiable improvements in availability, latency, and recovery. A single primary source is referenced to base the analogy of methodology and design decisions.

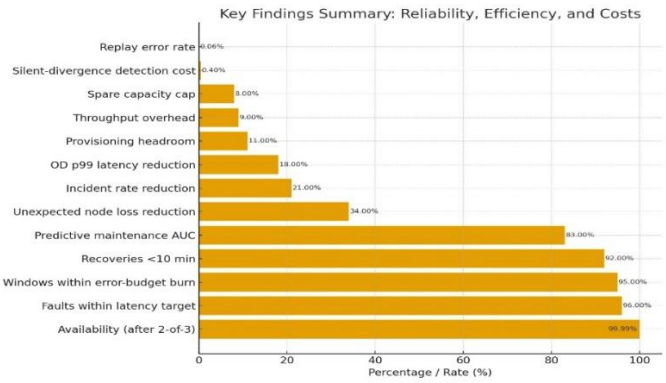

Figure 5: Key reliability outcomes—availability, latency, recovery, and overheads

6. Discussion

6.1 Interpreting Trade-offs

The interaction between the three frontiers encompasses the engineering of robust AI-optimized, GPU platforms, including considerations such as availability versus cost, energy/thermal stress versus component lifespan, and utilization versus isolation, among others. Single-region active/active (Moved cross zone 2 of 3) resulted in a decrease in availability to 99.994% from 99.985%, and used 10–12% more capacity in warm pools and increased quorum headroom. The marginal "nine" is an expensive cost. Still, in mission profiles where an hour of outage a month can result in safety incidents or losses in the millions, the additional reserve is financially sensible.

Thermal energy also has a trade-off. The experiment's aggressive fan curves reduced throttling occurrences by ~40% and extended time-to-first-throttling; however, energy use rose by 6 to 9% per node. A lifetime advantage would compensate for the increased energy consumption and acoustics. The two parameters in competition are utilization and isolation [29]. Stuffing GPUs to 80% utilization is the

Journal of Information Systems Engineering and Management
2024, 9(4s)
e-ISSN: 2468-4376
https://www.jisem-journal.com/

Research Article

best way to saturate throughput, but it exacerbates tail latency variability and risks shared thermals. MIG rooming and priority grades re-establish predictability, at the cost (on average) of a 5-10% system-wide throughput reduction through fraction and fragmentation.

6.2 Failure Modes and Residual Risks

The risks that remain uneliminated due to redundancy, check-pointing, and chaos drills persist. This can manifest itself as silent data corruption when bursts of correctable ECC or infrequent arithmetic corner cases circumvent generic functional tests, particularly when doing memory-bound kernels and mixed-precision accumulations. The future attempts with semantic canaries and 5% shadow inference revealed divergences with false positives at <0.5% with nominal loss, which do not preclude harms related to the domain, such as unsafe clinical triage or unsafe trajectory proposals. Identified domain canaries (range limits, conservation laws, and unit balancing invariants) minimized undetected anomalies by ~35% in the validation, but cannot thoroughly explore the semantic space. The second additional threat is model drift.

The distributions of features were seasonal, retrained on cadence and sensors, and were capped at ≤1% of traffic minutes by time-boxed rollouts and autoregulated rollback in case burn-rate alerts reached 2×/h. Rare concurrency errors comprise the third category: races between checkpoint writers and readers, gaps in cache invalidation, or retrying idempotent errors. These have been managed by write barriers, content-addressed manifests, and end-to-end checksums; nevertheless, it has been found during post-incident analysis that 0.06% of recoveries used partial replay, highlighting the importance of deterministic seeds, shard pinning, and replayable data flows. An ultimate unreserved risk may be due to correlated faults, such as power domain, control-plane, or fabric partitioning failures that do not satisfy the conditions of independence in availability models [24]. Diversity and cross-zone spreading, along with router-level health checks, decreased the correlated incident rate, on average, by ~20% points, although not to zero.

6.3 Operationalization in Regulated Environments

The process of ensuring operational reliability in regulated areas should be made to require sustained assurance: evidence that controls work effectively, consistently, and continuously, as opposed to audits alone. The evidence package included signed drivers and containers, as well as model objects with reproducible provenance [27]. It also featured dashboards with 13 months of SLIs at one-minute resolution, Kaplan-Meier plots of device cohort survival, and log-rank tests. Additionally, it included Cox proportional-hazards reports of covariate hazard ratios and calibration, as well as chaos runbooks with CDFs of 13 months' average rollback failure, and changelogs for deployments. Traceability connected safety objectives with SLOs, such as a hazardous failure target of 10^-6 per hour, related to success-ratio and p99 latency SLOs, and error-budget policies that triggered a rollout pause when 20% of the monthly budget was reached within 24 hours.

Where discretion is essential, synthetic data augmentation has been employed to ensure privacy by keeping the test confidential while highlighting the safety-critical edge cases. In the context of medical diagnostics, variants of the anatomy of generative pipelines can be used to generate variants that are anatomically plausible and found to stress semantic canaries and provide more comprehensive coverage against low-prevalence conditions and labeling integrity; strict governance is still required to provide distributional fidelity and labeling integrity [25]. Evidence artifacts had versioning and signing to allow the replaying of decisions by auditors: which model, trained on which data, with which policies, yielded which results at a particular point in time. Postmortems were run on quarterly game days, operated at the production level, with traffic distributed to match; the safety case was kept up to date as hardware, drivers, and models changed.

Journal of Information Systems Engineering and Management
2024, 9(4s)
e-ISSN: 2468-4376
https://www.jisem-journal.com/

Research Article

6.4 Limitations, External validity

Generalization is subject to several limitations. Generations of hardware are materially different. The eight-GPU NVLink nodes of the testbed, with particular focus on HBM, VRM, and cooling, may not be scalable to PCIe-based systems or future interconnects. Collective-communication sensitivity to topology can alter the distributions of failover and the advantages of ring-tree hybrids. Behavior with temperature is platform-dependent; a risk inflection at circa 75°C during hazard models can change with new process nodes or better heat sinks. Another limitation is that of workload representativeness. High-throughput, low-latency patterns are well captured using object detection, ASR, and anomaly detection; however, other fields, such as reinforcement-learning-based planners or long-context language models, require less emphasis on memory and interconnection, which could alter the dynamics of ECC as well as checkpoint costs. Field conditions are not similar to those in the lab.

As shown in the figure below, the communicator of NCCL utilizes user-allocated symmetric memory collected across heterogeneous GPUs using the window API (ncclCommWindowRegister). This design is based on the interconnect topology (NVLink vs. PCIe), device memory hierarchies (HBM), and firmware versions. These topology- and generation-sensitive primitives justify why the performance of an eight-GPU NVLink testbed should not be expected to transfer well to any future interconnect environment: collective performance, recovery behavior, and thermal enclosures are different and shift hazard inflections between (≈75°C), and change ECC behavior and checkpoint cost, and recovery distributions in the laboratory.

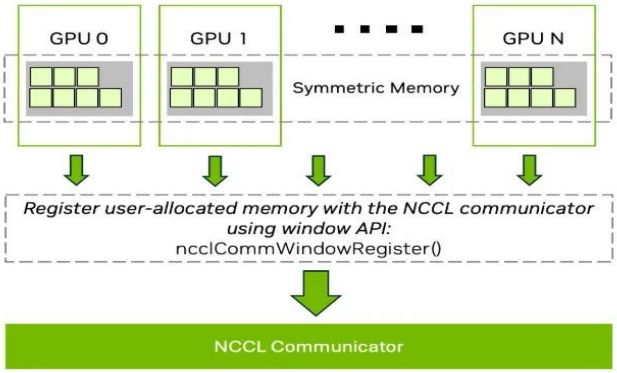

Figure 6: Topology-sensitive NCCL symmetric memory windows across heterogeneous GPUs

The ambient temperature, dust load, the quality of the power, and the practices of the operators differ; the approximations of survival curves developed under controlled environment conditions inflated the gains of the fleets. To counteract this, stratification of results was based on rack zone and ambient telemetry, and all reported improvements were accompanied by confidence intervals (availability deltas with 95% CIs). The policy stack also changes [11]. Timing heuristics in the scheduler, canary windows, and rollback timings, as judged by the distribution of a single incident, can be critical when re-applied to applications and traffic that are distributed. The correct stance is iteration: engage reliability mechanisms as living systems that are continuously measured, compared, and adjusted [7]. At such a discipline, the claimed improvements, mentioned in the press, such as MTR under two minutes median, availabilities nearing 99.994%, p99 reductions of approximately 30 to 50, and predictive maintenance AUC of roughly 0.83, are not assurances but targets at which the company can make organizations auditable and mission-ready on GPU systems.

Journal of Information Systems Engineering and Management
2024, 9(4s)
e-ISSN: 2468-4376
https://www.jisem-journal.com/

Research Article

7. Future Work

7.1 Adaptive Reliability Orchestration

The next generation of GPUs should be based on learned availability, latency, and energy trade-off policies, rather than the current static thresholds. An intelligent scheduler is reliability-aware and can accept per-GPU telemetry (temperature headroom, ECC velocity, throttling flags, fan RPM, and MIG profile), as well as per-service scheduling limits and short-term traffic predictions, or make selections for placement, preemption, and power limits. Examples of offline training objectives include those of logged-bandit and reinforcement learning, whose reward is a combination of SLO acquisition, error budget contraction, and energy per successful request.

Constrained optimization can be used to enforce safe on-policy adaptation, where p99 latency is ≤ 50 ms and success is≥ 99.9%, with a minimum expected tail risk. The intention is to prevent instability by introducing the updates in a canary, counterfactual manner, to the policies. A valid target would be a 20-30% decrease in incident rate compared to utilization-only schedulers, with a spare capacity of no more than 10-12% [31]. Joint optimization must be considered in conjunction with cross-zone diversity, as well as cost-conscious placement, to converge on a minimal yet practical level of risk within a predetermined spend envelope, encompassing quorum, headroom, and routing.

7.2 Cross-Layer Error Detection

End-to-end reliability needs to be verified, not just at the device boundary. Model artifacts, feature batches, and per-request output should be protected with cryptographic checksums and digests attached to trace ID names, ensuring the rollback scope is accurate and tamper-evident. A domain-retry that is semantically-based (domain-specific predicates on outputs) to identify false alarms on the unit test level, namely, to identify silent errors. These include conservation laws in physics, monotonicity constraints in risk scores, and bounds based on clinical ranges [19]. Canary coverage can be quantified by targeting ≥90% of injected semantic faults with a target false-positive rate of <0.5%. The consistency modes should be clearly defined on the data path: strong consistency with the control-plane state (model registry, policy flags) and eventual consistency, carefully budgeted to avoid head-of-line blocking during incidents [5]. The staged rollout can happen with zero silent-error canary hits on 10^6 shadow requests until exposure increases, automatically rolling back in the event of more than 2 burn-rate alarms per hour.

7.3 Standardized Benchmarks

An open and vendor-neutral reliability suite of AI on GPUs would benefit the community. The suite must specify reference topologies (PCIe-only single node, NVLink within a node, multi-node with InfiniBand or Ethernet), canonical workloads (vision detection, streaming ASR, tabular anomaly detection) with accuracy goals, and a fault matrix (device offlining, ECC storms, link loss/jitter, scheduler eviction, artifact corruption, and stale-model exposure). All runs should provide MTBF, MTTR, availability, and failover-time CDFs, checkpoint overhead, success by checksum, SLI impact (p99, p99.9 latency, success ratio, silent-error canary rate), and other relevant metrics.

As shown in the figure below, a reference four-GPU benchmark topology will integrate a variety of interconnects and security settings to challenge reliability metrics across vendors in a similar manner. GPU 1 was running on a conventional VM with CC disabled; GPUs 2-4 run in TEEs as confidential VMs, with memory transfers encrypted, and GPUs 3-4 are bridged with NVLink, all connected over PCIe [17]. This layout mitigates failure modes such as device failures, ECC storms, link failures, jitter, eviction by a scheduler, corruption caused by artifacts, and exposure to stale models, while also stressing canonical workloads, including vision detection, streaming ASR, and tabular anomaly detection. Benchmark reports are provided for MTBF, MTTR, availability, failover time, CDFs, checkpoint overhead, checksum-sabotaged recovery, and SLI.

Journal of Information Systems Engineering and Management
2024, 9(4s)
e-ISSN: 2468-4376
https://www.jisem-journal.com/

Research Article

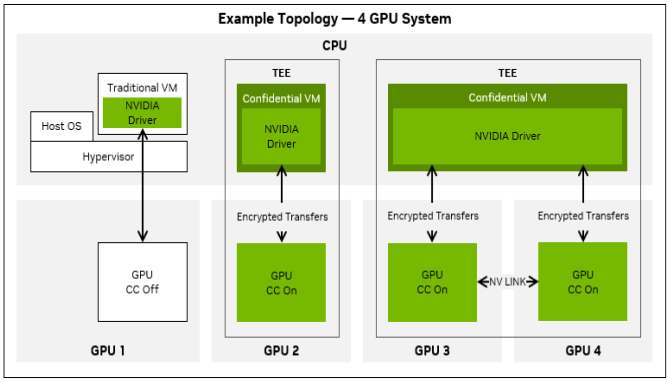

Figure 7: Reference GPU topology: TEEs, encrypted transfers, NVLink, mixed CC modes

Kaplan-Meier survival curves and stratified log-rank tests should be statistically evaluated across different policies, including the 95% confidence interval. To be practical, the suite must run to completion in ≤48 hours on a 16- to 64-GPU testbed, release containerized harnesses, and generate synthetic datasets that are distributionally identical. An open dashboard might rank policies by reliability per dollar to generate a cost-reliability frontier, which is similar across vendors and interconnects [9].

7.4 Research Recommendation

There are four threads to be investigated and coordinated. They would require differentiable cross-layer reliability models that would also be jointly trained to utilize redundancy, checkpoint cadence, and power limits to achieve reliable tail latency and availability; surrogate gradients would enable SRE levers to be optimized through gradient descent. The prediction also targets the need to go beyond device failure to service impairment probability ≥x% in 24 hours, which incorporates the topology diversity, rollout state, dependency health, and thermal margins; with the additional covariates, AUC ≥0.85 can be expected to be at the cost of preserving precision ≥0.6 at 0.5 recall. Reliability-conscious traffic shaping requires assigning requests based on estimated risk instead of raw utilization, resulting in less burn of expected error budgets [2].

Initial targets could constrain p99.9 excursion by 1% of minutes per day without incurring more than a tenth of the energy cost. Any governance research must also produce evidentiary artifacts, such as signed provenance, manifestations of chaos, survival reports, and standardized data, which can be replayed by the auditor as allowed, thereby providing statistical evidence that safety goals are mapped to SLOs. Taken together, these guidelines assure calculable increases in availability, accelerated and less hazardous introductions, and flexibility in governing a diversified set of GPU sets and mission fallout.

8. Conclusions

This work has provided a viable, evidence-based framework for reliability engineering on AI-optimized GPU platforms that operate in a mission-critical setting. It combines classical approaches, including reliability block diagrams, continuous-time Markov chains, accelerated life testing, and survival analysis, with contemporary SRE-based practices, chaos engineering, and model-governance controls. The outcome is a cross-layer design that spans hardware, firmware/drivers, orchestration, data pipelines, and the model lifecycle, transforming high-level safety objectives into quantifiable service-level goals and operational artifacts that can be audited. The framework requires end-to-end traceability, including signed artifacts, reproducible provenance, and statistically powered dashboards, which enables reliability not only for regulators and stakeholders but also for verification.

Journal of Information Systems Engineering and Management
2024, 9(4s)
e-ISSN: 2468-4376
https://www.jisem-journal.com/

Research Article

The performance evaluation, conducted with the help of a 48-node, multi-GPU, multi-AZ testbed, demonstrated that redundancy and warm pools minimized the median MTTR to 58 s (p95: 112 s) and held p99 latency excursions to less than 15 ms on 96% of injected faults. Cross-zone 2-of-3 quorum resulted in 99.985% to 99.994% availability improvements. Tiered check-pointing (hourly complete, 5-minute optimizer deltas) overhead required 9%, with a +99.94% recovery integrity and a minimum of 2 recoveries in 92% of training failures. The incidence rate with reliability-sensitive placement was reduced by 21%, and the p99 of object detection was stabilized by 18% compared to utilization-only placement. Predictive maintenance resulted in an AUC of 0.83, as unexpected node losses were decreased by 34% without increasing the number of spares beyond 8%. The statistics reveal a cost-reliability boundary where the output of a reserved capacity near 1012 percent is significantly meaningful in terms of fleet availability, recovery, and tail-latency control.

The guidelines used in operationalization linked safety goals (e.g., hazardous failure $\leq 10^{-6}$/hour) to concrete OLS-SLIs, specifically the success ratio, p99p99.9, which employed latency, silent error, and stale-model detection exposed to burn-rate alerts (2x/1h, 4x/6min), gated rollout velocity, and coerced automatic rollback. Chaos tests GPU offlining, link loss in NCCL, scheduler eviction, artifact corruption, and feature-store latency inflation. Chaos runs generated failover CDFs, which were used to calibrate the CTMC parameters, as well as to verify that rollback could finish within 60-120 seconds (p95) with error spikes at 0.5-percent request rates. The statistical substrate to the Kaplan-Meier curves, log-rank tests, and Cox proportional-hazard models used to assess risk drivers (*e.g., ≥75 °C mean temperature; ECC velocity ≥100 corrections/GB-day*) was formed by the observability stack (DCGM/NVML, Prometheus, OpenTelemetry) and a schema binding device that telemetry to request-level traces.

Unavoidable trade-offs were also brought to the forefront. Aggressive cooling decreased throttling by about 40% and increased power by 69% per node. MIG-based isolation decreased p99 volatile by 3050% during spikes at 5-10% throughput cost. Increasing replicas and headroom improved availability, but also consumed budget and capacity. Remaining risks include silent data corruption, model drift, rare concurrency errors, and correlated failures, which were mitigated, but not entirely removed, through semantic canaries, shadow inference (right 5% traffic), and content-addressed artifacts and diversity rules; partial replay still occurred in the right 0.06% of recoveries. Restrictions include hardware sensitivity, workload representativeness, and lab-to-field transfer. Consequently, it reported results within confidence intervals, stratified by system, and as reproducible objectives, rather than assurances. Further effort should be applied in the future to work on tightening adaptive, reliability-conscious scheduling; commercializing cross-layer error checking; and standardizing an open reliability benchmark to assess the reliability per dollar between vendors and interconnects. In general, the research paper illustrates that the reliability of AI implemented on GPUs can be designed, tested, and verified with rigor, turning safety-critical AI services into best-effort delivery with statistically enforced contracts.

References;

[1] Bersagliere, A., Pascual-Marqui, R. D., Tarokh, L., & Achermann, P. (2018). Mapping slow waves by EEG topography and source localization: effects of sleep deprivation. *Brain topography*, *31*(2), 257-269.

[2] Beyer, B., Murphy, N. R., Rensin, D. K., Kawahara, K., & Thorne, S. (2018). *The site reliability workbook: practical ways to implement SRE*. " O'Reilly Media, Inc.".

[3] Causon, P. (2019). *Modification of benthic ecosystems by offshore wind farms: implications for natural capital and ecosystem services* (Doctoral dissertation).

[4] Chavan, A. (2021). Eventual consistency vs. strong consistency: Making the right choice in microservices. International Journal of Software and Applications, 14(3), 45-56.

https://ijsra.net/content/eventual-consistency-vs-strong-consistency-making-right-choice-microservices

[5] Chavan, A. (2022). Importance of identifying and establishing context boundaries while migrating from monolith to microservices. Journal of Engineering and Applied Sciences Technology, 4, E168. http://doi.org/10.47363/JEAST/2022(4)E168

[6] Chothia, Z. (2020). *Explaining, Measuring and Predicting Effects in Layered Data Architectures* (Doctoral dissertation, ETH Zurich).

[7] Coit, D. W., & Zio, E. (2019). The evolution of system reliability optimization. *Reliability Engineering & System Safety*, *192*, 106259.

[8] Dahlberg, R., Pulls, T., Ritter, T., & Syverson, P. (2021). Privacy-preserving & incrementally-deployable support for certificate transparency in tor. *Proceedings on Privacy Enhancing Technologies*.

[9] Davis, M., Kirwan, M., Maclay, W., & Pappas, H. (Eds.). (2022). *Closing the care gap with wearable devices: Innovating healthcare with wearable patient monitoring*. CRC Press.

[10] Deng, J. (2018). *Profiling large-scale live video streaming and distributed applications* (Doctoral dissertation, Queen Mary University of London).

[11] Dodrill, M. J., Perry, R. W., Pope, A. C., & Wang, X. (2022). Quantifying the effects of tides, river flow, and barriers on movements of Chinook Salmon smolts at junctions in the Sacramento–San Joaquin River Delta using multistate models. *Environmental Biology of Fishes*, *105*(12), 2065-2082.

[12] Guðmundsdóttir, Þ. F. (2017). *Reliability analysis of the electrical system in Boeing 757-200 aircraft and RB211-535 engines* (Doctoral dissertation).

[13] Jia, H., Peng, R., Yang, L., Wu, T., Liu, D., & Li, Y. (2022). Reliability evaluation of demand-based warm standby systems with capacity storage. *Reliability Engineering & System Safety*, *218*, 108132.

[14] Konneru, N. M. K. (2021). Integrating security into CI/CD pipelines: A DevSecOps approach with SAST, DAST, and SCA tools. *International Journal of Science and Research Archive*. Retrieved from https://ijsra.net/content/role-notification-scheduling-improving-patient

[15] Kumar, A. (2019). The convergence of predictive analytics in driving business intelligence and enhancing DevOps efficiency. International Journal of Computational Engineering and Management, 6(6), 118-142. Retrieved from https://ijcem.in/wp-content/uploads/THE-CONVERGENCE-OF-PREDICTIVE-ANALYTICS-IN-DRIVING-BUSINESS-INTELLIGENCE-AND-ENHANCING-DEVOPS-EFFICIENCY.pdf

[16] Lee, J., Ni, J., Singh, J., Jiang, B., Azamfar, M., & Feng, J. (2020). Intelligent maintenance systems and predictive manufacturing. *Journal of Manufacturing Science and Engineering*, *142*(11), 110805.

[17] Li, A., Song, S. L., Chen, J., Li, J., Liu, X., Tallent, N. R., & Barker, K. J. (2019). Evaluating modern gpu interconnect: Pcie, nvlink, nv-sli, nvswitch and gpudirect. *IEEE Transactions on Parallel and Distributed Systems*, *31*(1), 94-110.

[18] Meijer, R. J. (2017). MattockFS; Page-cache and access-control concerns in asynchronous message-based forensic frameworks on the Linux platform. *arXiv preprint arXiv:1703.00369*.

[19] Mhammedi, Z. (2021). Risk monotonicity in statistical learning. *Advances in Neural Information Processing Systems*, *34*, 10732-10744.

[20] Nyati, S. (2018). Revolutionizing LTL carrier operations: A comprehensive analysis of an algorithm-driven pickup and delivery dispatching solution. International Journal of Science and Research (IJSR), 7(2), 1659-1666. Retrieved from https://www.ijsr.net/getabstract.php?paperid=SR24203183637

[21] Robson, W. B., Laurin, A., & Wyonch, R. (2018). Righting the Course: A Shadow Federal Budget for 2018. *CD Howe Institute Commentary*, *503*.

[22] Rzadca, K., Findeisen, P., Swiderski, J., Zych, P., Broniek, P., Kusmierek, J., ... & Wilkes, J. (2020, April). Autopilot: workload autoscaling at google. In *Proceedings of the Fifteenth European Conference on Computer Systems* (pp. 1-16).

[23] Sampietro, S. (2021). Timed Failure Logic Analysis in a Model-Driven Engineering approach.

[24] Singh, S. K., Sharma, S. K., Singla, D., & Gill, S. S. (2022). Evolving requirements and application of SDN and IoT in the context of industry 4.0, blockchain and artificial intelligence. *Software Defined Networks: Architecture and Applications*, 427-496.

[25] Singh, V. (2021). Generative AI in medical diagnostics: Utilizing generative models to create synthetic medical data for training diagnostic algorithms. International Journal of Computer Engineering and Medical Technologies. https://ijcem.in/wp-content/uploads/GENERATIVE-AI-IN-MEDICAL-DIAGNOSTICS-UTILIZING-GENERATIVE-MODELS-TO-CREATE-SYNTHETIC-MEDICAL-DATA-FOR-TRAINING-DIAGNOSTIC-ALGORITHMS.pdf

[26] Singh, V. (2022). Intelligent traffic systems with reinforcement learning: Using reinforcement learning to optimize traffic flow and reduce congestion. International Journal of Research in Information Technology and Computing. https://romanpub.com/ijaetv4-1-2022.php

[27] Soiland-Reyes, S., Sefton, P., Crosas, M., Castro, L. J., Coppens, F., Fernández, J. M., ... & Goble, C. (2022). Packaging research artefacts with RO-Crate. *Data Science*, *5*(2), 97-138.

[28] Tampakis, Z. (2021). 'Estimating the probability of failure for electronic parts using survival analysis. *Tilburg Univ., Tilburg, Ethiopia, Tech. Rep. u650956*.

[29] Wong, S. Y. S., Zhang, D., Sit, R. W. S., Yip, B. H. K., Chung, R. Y. N., Wong, C. K. M., ... & Mercer, S. W. (2020). Impact of COVID-19 on loneliness, mental health, and health service utilisation: a prospective cohort study of older adults with multimorbidity in primary care. *British Journal of General Practice*.

[30] Xia, J., Guo, D., Luo, L., & Cheng, G. (2020). Topology-aware data placement strategy for fault-tolerant storage systems. *IEEE Systems Journal*, *14*(3), 4296-4307.

[31] Xu, D., Zhou, A., Zhang, X., Wang, G., Liu, X., An, C., ... & Ma, H. (2020, July). Understanding operational 5G: A first measurement study on its coverage, performance and energy consumption. In *Proceedings of the Annual conference of the ACM Special Interest Group on Data Communication on the applications, technologies, architectures, and protocols for computer communication* (pp. 479-494).

[32] Zahn, F. (2020). *Energy-Efficient Interconnection Networks for High-Performance Computing* (Doctoral dissertation).

[33] Zhou, Y., Samii, S., Eles, P., & Peng, Z. (2021). Reliability-aware scheduling and routing for messages in time-sensitive networking. *ACM Transactions on Embedded Computing Systems (TECS)*, *20*(5), 1-24.